

## Sub-threshold $\text{Ca}^{2+}$ waves

**J W Shuai and P Jung<sup>1</sup>**

Department of Physics and Astronomy, Quantitative Biology Institute,  
Ohio University, Athens, OH 45701, USA  
E-mail: [jungp@ohio.edu](mailto:jungp@ohio.edu)

*New Journal of Physics* **5** (2003) 132.1–132.20 (<http://www.njp.org/>)

Received 2 May 2003

Published 10 October 2003

**Abstract.** In this paper we consider a model for intracellular  $\text{Ca}^{2+}$  waves where the ion channels (excitability) is distributed in spatially distinct clusters. We report that channel noise in conjunction with spatial clustering can result in the onset of spatially and temporally extremely coherent  $\text{Ca}^{2+}$  signals at levels of stimulant well below the threshold of  $\text{Ca}^{2+}$  oscillations for homogeneously distributed channels. The physiological significance of this phenomenon is strongly enhanced cellular  $\text{Ca}^{2+}$ -signalling capability with few agonist molecules binding.

### Contents

<b>1</b>	<b>Introduction</b>	<b>2</b>
<b>2</b>	<b>The model</b>	<b>3</b>
<b>3</b>	<b>The limit of large diffusion coefficients</b>	<b>5</b>
<b>4</b>	<b>Sub-threshold coherent <math>\text{Ca}^{2+}</math> oscillations</b>	<b>7</b>
<b>5</b>	<b>Optimal clustering</b>	<b>13</b>
<b>6</b>	<b>Discussion and conclusion</b>	<b>16</b>
	<b>Acknowledgment</b>	<b>18</b>
	<b>Appendix A. The stochastic calcium flux density through clustered <math>\text{IP}_3\text{Rs}</math> (equation (4))</b>	<b>18</b>
	<b>Appendix B. The deterministic calcium flux density through <math>\text{IP}_3\text{Rs}</math> (equation (7))</b>	<b>19</b>
	<b>References</b>	<b>20</b>

<sup>1</sup> Author to whom any correspondence should be addressed.

## 1. Introduction

Calcium ions are ubiquitous in cells as intracellular messengers [1].  $\text{Ca}^{2+}$  participates in a wide range of processes such as triggering the development and differentiation of cells after fertilization, contracting muscle cells and triggering injury response in epithelia cells to name but a few. Different genes can be activated by varying the frequency or amplitude of  $\text{Ca}^{2+}$  signals [2, 3]. A very high concentration of  $\text{Ca}^{2+}$  is no longer a signal of life, but a signal of death, and is invariably involved in cell death [1].

The release of calcium ions from internal stores, e.g. the endoplasmic reticulum (ER) or sarcoplasmic reticulum (SR), into the cytosol plays a central role for calcium signals in many excitable and non-excitable cells. Inositol triphosphate receptors ( $\text{IP}_3\text{R}$ ) and ryanodine receptors (RyR) represent the two major types of intracellular calcium release channels on the membrane of the ER or SR. Agonist binding to G-protein coupled receptors in the cell membrane results in production of the second messenger inositol 1,4,5-triphosphate ( $\text{IP}_3$ ).  $\text{IP}_3$  diffuses from the cell membrane to the nearby ER and binds to an  $\text{IP}_3\text{R}$  which can open and release  $\text{Ca}^{2+}$  from the ER which in turn can open more  $\text{IP}_3$  channels (calcium-induced calcium release (CICR)) and thus cause a fast release of  $\text{Ca}^{2+}$  from internal stores. This  $\text{Ca}^{2+}$  signal is terminated when the intracellular concentration becomes large and the  $\text{Ca}^{2+}$  pumps remove  $\text{Ca}^{2+}$  from the intracellular space into the ER and out of the cell. This constitutes a  $\text{Ca}^{2+}$  signal that is repetitive if the concentration of  $\text{IP}_3$  is larger than a threshold. Similarly to neuronal signalling, it is believed that the frequency carries the main information in the  $\text{Ca}^{2+}$  signal. Thus,  $\text{IP}_3$  signals below the threshold are not coded in a  $\text{Ca}^{2+}$  signal.

Recently, it has been revealed that in many cells the cytoplasm does not act as a continuous, homogeneous excitable medium to generate  $\text{Ca}^{2+}$  release. Instead,  $\text{Ca}^{2+}$  liberation occurs at discrete, functional release sites, spaced a few micrometres apart, that generate localized, elementary  $\text{Ca}^{2+}$  signalling events, termed puffs or sparks [4, 5]. The puff sites are believed to be formed by clusters of  $\text{IP}_3$  release channels ( $\text{IP}_3\text{Rs}$ ), distributed on the ER membrane. Each cluster is comprised of a few tens of intact  $\text{IP}_3\text{Rs}$  [6, 7]. The spontaneous opening of one channel, caused by thermal fluctuations in the configuration of the channel protein, may cause more channels to open via CICR and generate local  $\text{Ca}^{2+}$  release events with a broad range of amplitudes, lifetimes and interpuff intervals [8]–[10].  $\text{Ca}^{2+}$  puffs function as elementary building blocks through which various  $\text{Ca}^{2+}$  waves can be generated [11]. By coordinating the spatially discrete  $\text{Ca}^{2+}$  release events, a  $\text{Ca}^{2+}$  wave can be generated that spreads throughout the cell [12, 13]. Such intracellular waves can spread into neighbouring cells mediated by intra- and extracellular messengers, resulting in intercellular waves [14]. Intracellular or intercellular  $\text{Ca}^{2+}$  signals can display spatially and temporally complex patterns. The temporal patterns of  $\text{Ca}^{2+}$  observed in a variety of cells include oscillations or repetitive spikes. Some cells, most notably *Xenopus* oocytes, also exhibit interesting spatial patterns, including propagating waves, target or spiral patterns [12, 13].

The calcium signals feature a hierarchical organization, from highly localized blips [15] and puffs to intracellular or intercellular wave. The hierarchical calcium signals can regulate many different cellular processes, locally or globally. For example,  $\text{Ca}^{2+}$  sparks in smooth muscle cells that arise locally and near the plasma membrane activate potassium channels, causing the muscle to relax. But when localized release events deeper in the cell are coordinated to create a global  $\text{Ca}^{2+}$  signal, the muscle contracts [1]. The spatially clustered  $\text{IP}_3\text{R}$  organization enables  $\text{Ca}^{2+}$  to activate opposing cellular responses in the same cell but at different levels.

Experimentally controllable parameters in cells are the  $\text{IP}_3$  concentration and calcium diffusion coefficient  $D$ . The  $\text{IP}_3$  concentration can be stimulated and adjusted by the binding of extracellular agonists such as hormones or neurotransmitters to receptors in the membrane [8] or more precisely by photo-release of caged  $\text{IP}_3$  [3]. The  $\text{Ca}^{2+}$  diffusion coefficient can be controlled by intracellularly loading with  $\text{Ca}^{2+}$  buffer EGTA. Depending on the  $\text{IP}_3$  concentration and the  $\text{Ca}^{2+}$  diffusion, different patterns of  $\text{Ca}^{2+}$  release can be observed. Puffs are easily observed with the loading of EGTA even at large  $\text{IP}_3$  concentration [16, 10]. It has been shown that in *Xenopus* oocyte,  $\text{Ca}^{2+}$  puffs can be observed in narrow regions at low  $\text{IP}_3$  concentration in the absence of EGTA [5, 8]. At slightly higher concentrations of  $\text{IP}_3$ , abortive calcium waves travel only short distances [5]. At high  $\text{IP}_3$  concentration, a large tide of  $\text{Ca}^{2+}$  release with no repetitive  $\text{Ca}^{2+}$  waves are observed [13]. At intermediate concentrations of  $\text{IP}_3$ , repetitive  $\text{Ca}^{2+}$  waves are obtained.

Numerically, the intracellular  $\text{Ca}^{2+}$  waves are widely simulated by approximating the  $\text{Ca}^{2+}$  channels as deterministic and spatially continuous source terms [17]–[19]. These reaction–diffusion models explain the observed  $\text{Ca}^{2+}$  patterns as nonlinear waves in an excitable, oscillatory, or bistable medium. To elucidate the transition from localized to travelling patterns, the clustered distribution of the  $\text{Ca}^{2+}$  release has been taken into account [20]–[23]. With deterministic models of clustered  $\text{Ca}^{2+}$  release, novel forms of waves such as pinned waves, saltatory spreading wave, and abortive wave have been observed [22, 23]. The simulation shows that the speed of spreading waves is proportional to the diffusion constant of calcium, rather than its square root in the continuous medium case.

The observation of localized stochastic  $\text{Ca}^{2+}$  puffs created by the cluster of a few tens of  $\text{IP}_3\text{Rs}$  [8]–[10], however, suggests that stochastic effects are relevant for  $\text{Ca}^{2+}$  wave propagation and need to be taken into account. Recently, several such models with stochastic and spatially discrete  $\text{IP}_3\text{R}$  sources have been proposed. Keizer and Smith [24] introduced a spatially one-dimensional, stochastic model with a clustered distribution of  $\text{Ca}^{2+}$  release channels for cardiac myocytes, showing a transition from spark to wave. Another stochastic model for cells where  $\text{Ca}^{2+}$  is released from the ER, put forward by Falcke *et al* [25], is based on the stochastic version of the DeYoung–Keizer model [26]. It shows a transition from spark to abortive wave to steady wave in one spatial dimension. A back-firing state is observed in a two-dimensional version of the model due to stochastic channel dynamics.

In this paper, we report on a novel phenomenon that occurs as consequence of the clustering and stochasticity of  $\text{IP}_3$  receptors. We find the onset of coherent oscillations well below the threshold of stimulation at which the spatially homogeneous model predicts  $\text{Ca}^{2+}$  oscillations. These oscillations occur in a small interval of  $\text{IP}_3$  concentrations at values of  $\text{Ca}^{2+}$  diffusion coefficients that are slightly below typical values. It is further remarkable that the spatial and temporal correlations of these sub-threshold oscillations exceed significantly those in the regime of deterministic oscillations. This phenomenon may be related to  $\text{Ca}^{2+}$  wave nucleation [27].

## 2. The model

$\text{Ca}^{2+}$  is stored in internal stores, most notably the ER. It enters the cytosol via channels in the plasma membrane of the ER. The flux through these channels is determined by the concentration of  $\text{Ca}^{2+}$  in the cell and by that of the messenger  $\text{IP}_3$ . According to the DeYoung–Keizer model [26] the  $\text{IP}_3$  receptor channels ( $\text{IP}_3\text{Rs}$ ) consist of four subunits, where three have to be activated for the channel to be open. Each subunit has three binding sites, one for  $\text{IP}_3$  and two for  $\text{Ca}^{2+}$ .

One  $\text{Ca}^{2+}$  binding site activates the subunit, while the other  $\text{Ca}^{2+}$  binding site inactivates the subunit. Since there is a vast difference in the timescale of these three binding processes, one can replace the occupancy of the fast  $\text{IP}_3$  binding and  $\text{Ca}^{2+}$  activation binding sites by their average values and only consider dynamically the slow inactivation process. Such an elimination process results in a two-variable model for the receptor dynamics [28] which we adopt in this paper. The cell is modelled as a two-dimensional sheet with two domains, the cytosol and the ER. The ER is homogenized over the entire cell so that each spatial location in the cell belongs to both domains. The sheet is assumed thin so that the  $\text{Ca}^{2+}$  concentrations in the cytosol and the ER are homogeneous across the sheet. The two domains interact via the release of  $\text{Ca}^{2+}$  from ER into the cytosol through discretely distributed receptor channels and subsequent diffusion and re-uptake by the ER. The smallness of the release clusters requires stochastic modelling of their conductance. All intracellular  $\text{Ca}^{2+}$  buffers are assumed to be fast so that their presence can be modelled by an effective diffusion coefficient  $D$  (values have been experimentally determined). The  $\text{IP}_3$ Rs are distributed in clusters positioned on a regular grid. The total number of  $\text{IP}_3$ Rs is considered fixed while they can be distributed differently, ranging from numerous small clusters (with only one channel each) at a small distance to few large clusters at larger distances. The equation for the intracellular  $\text{Ca}^{2+}$  concentration  $[\text{Ca}^{2+}]$  is given by

$$\frac{d[\text{Ca}^{2+}](x, y)}{dt} = D\nabla^2[\text{Ca}^{2+}](x, y) + \sum_i f(x, y)J_{\text{Channel}}^{(i)} - J_{\text{Pump}} + J_{\text{Leak}} \quad (1)$$

where  $\text{Ca}^{2+}$  can diffuse in the cytosol with diffusion constant  $D$ . There are three fluxes of  $\text{Ca}^{2+}$  between the cytosol and the ER. The terms  $J_{\text{Channel}}^{(i)}$  describe the  $\text{Ca}^{2+}$  fluxes through the release channels localized in small intervals around the discrete sites  $(x_i, y_i)$  where the form function  $f(x, y)$  is nonzero. The release sites  $(x_i, y_i)$  are organized on a square lattice with variable lattice constant (see below). The flux  $J_{\text{Pump}}$  describes the  $\text{Ca}^{2+}$  re-uptake through SERCA pumps, and  $J_{\text{Leak}}$  describes leak flux. The pumps and leaks are assumed homogeneously distributed over the plasma membrane of the ER and their fluxes are given by

$$J_{\text{Pump}} = v_p \frac{[\text{Ca}^{2+}]^2}{k^2 + [\text{Ca}^{2+}]^2} \quad (2)$$

$$J_{\text{Leak}} = v_L([\text{Ca}^{2+}]_{\text{ER}} - [\text{Ca}^{2+}]), \quad (3)$$

where  $[\text{Ca}^{2+}]_{\text{ER}}$  denotes the  $\text{Ca}^{2+}$  concentration in the ER.

For the channel flux, we use the stochastic version [29, 30] of the Li–Rinzel model [28], which is a reduction of the more detailed stochastic DeYoung–Keizer model [25] and accurate for processes on the timescale of seconds [31]. The channels are concentrated in clusters of less than  $0.5 \mu\text{m}$  diameter which is much smaller than the diffusion length of  $\text{Ca}^{2+}$  with a physiological diffusion constant of  $D \approx 20 \mu\text{m}^2 \text{s}^{-1}$ . This allows us to assume that the  $\text{Ca}^{2+}$  concentration is constant within the cluster (see also [6]) and to model the  $\text{Ca}^{2+}$  flux from the ER into the cytosol as a *point source* with a weight factor that describes the size of the source resulting in a  $\text{Ca}^{2+}$  flux through cluster  $(i)$ , given by

$$J_{\text{Channel}}^{(i)} = v_C m_\infty^3 n_\infty^3 N_{\text{open}}^{(i)} ([\text{Ca}^{2+}]_{\text{ER}} - [\text{Ca}^{2+}]), \quad (4)$$

where  $v_C$  contains the ratio of channel size and grid size (for details on this procedure see appendix A and [32]) and

$$m_{\infty} = \frac{[\text{IP}_3]}{[\text{IP}_3] + d_4} \quad (5)$$

$$n_{\infty} = \frac{[\text{Ca}^{2+}]}{[\text{Ca}^{2+}] + d_5},$$

where  $[\text{IP}_3]$  denotes the concentration of  $\text{IP}_3$ . The number of open channels of cluster  $(i)N_{\text{open}}^{(i)}$  is determined by Markov processes describing the state of each channel. The three subunits of the  $\text{IP}_3$  receptor result in three gates in the reduced model, with opening and closing rates  $\alpha_h$  and  $\beta_h$  given by

$$\alpha_h = ad_2 \frac{[\text{IP}_3] + d_1}{[\text{IP}_3] + d_3} \quad (6)$$

$$\beta_h = a[\text{Ca}^{2+}],$$

respectively. For small clusters  $N$  direct simulation of each subunit as Markov two-state processes, the least economical but most accurate method, can be carried through.

If a subunit is at time  $t$  in the inactivated state, the probability of activation during the time interval  $[t, t + \delta t]$  is given by  $\alpha_h \delta t$  where  $\alpha_h$  is the activation rate given in equation (6), while the probability of remaining in the inactivated state reads  $1 - \alpha_h \delta t$ . In order to decide whether the subunit remains inactivated or activates within the time interval  $\delta t$ , we draw a random number from a uniform distribution over the unit interval. If it is less than or equal to  $\alpha_h \delta t$ , the subunit is switched into the activated state, otherwise it remains in the inactivated state. If a subunit is at time  $t$  in the activated state, the probability of inactivation during the time interval  $[t, t + \delta t]$  is given by  $\beta_h \delta t$  where  $\beta_h$  is the inactivation rate (6), while the probability of remaining activated reads  $1 - \beta_h \delta t$ . To decide whether the subunit remains activated or de-activates, we again draw a random number from a uniform distribution over the unit interval. If it is less or equal to  $\beta_h \delta t$ , the subunit is switched into the inactivated state, otherwise it remains in the activated state. The release channel is open when all three subunits of a channels are activated. For larger numbers of channels per cluster more economical methods are available where the channels are categorized into groups with zero, one, two or three activated gates and only occupancy of these groups and their transitions are recorded (see e.g. [33]).

The concentration of  $\text{Ca}^{2+}$  in the ER, i.e.  $[\text{Ca}^{2+}]_{\text{ER}}$ , is set to the constant value of  $15 \mu\text{M}$ . The size of the cell simulated is  $60 \mu\text{m} \times 60 \mu\text{m}$ . The computer cell thus has the form of a mosaic of active and passive (still nonlinear) patches. Of critical importance is the diffusion constant of  $\text{Ca}^{2+}$  in the cytosol. Effective diffusion coefficients of  $\text{Ca}^{2+}$  in the cytosol reported in the literature [34] range from  $10$  to  $220 \mu\text{m}^2 \text{s}^{-1}$ . The other parameter values in the model are  $v_C = 0.6 \text{s}^{-1}$ ,  $v_P = 0.5 \text{s}^{-1}$ ,  $v_L = 0.001 \mu\text{M s}^{-1}$ ,  $[\text{Ca}^{2+}]_{\text{ER}} = 15.0 \mu\text{M}$ ,  $k = 0.1 \mu\text{M}$ ,  $a = 0.2 \mu\text{M}^{-1} \text{s}^{-1}$ ,  $d_1 = 0.13 \mu\text{M}$ ,  $d_2 = 1.05 \mu\text{M}$ ,  $d_3 = 0.94 \mu\text{M}$ ,  $d_4 = 0.13 \mu\text{M}$ , and  $d_5 = 0.08 \mu\text{M}$ . These parameters are modified from the original Li–Rinzel model [28]. The parameters have been chosen such that the resulting  $\text{Ca}^{2+}$  waves exhibit speeds that are consistent with experimental values in *Xenopus* oocyte.

The stochastic partial differential equations are solved by using a standard five point discretization scheme for the Laplacian in connection with a fully explicit solver. The accuracy has been tested by using smaller discretization intervals.

### 3. The limit of large diffusion coefficients

Although physiological values of the diffusion coefficient  $D$  of  $\text{Ca}^{2+}$  are between  $15$  and  $30 \mu\text{m}^2 \text{s}^{-1}$  we consider here the limit case when  $D$  is more than 10 times this value.

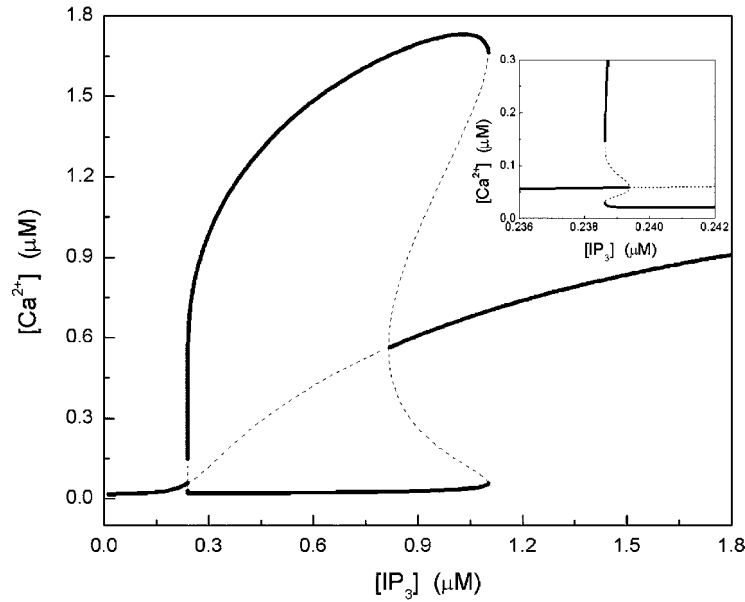


**Figure 1.** The bifurcation diagram of equation (7) is shown as a function of the  $\text{IP}_3$  concentration. For  $[\text{IP}_3] < 0.24 \mu\text{M}$  the  $\text{Ca}^{2+}$  concentration approaches a fixed point. Through subcritical Hopf bifurcations at  $[\text{IP}_3]^{\text{h1}} = 0.24 \mu\text{M}$  and  $[\text{IP}_3]^{\text{h2}} = 0.82 \mu\text{M}$  a stable limit cycle emerges for  $[\text{IP}_3]^{\text{sn1}} < [\text{IP}_3] < [\text{IP}_3]^{\text{sn2}}$  with  $[\text{IP}_3]^{\text{sn1}} = 0.24 \mu\text{M}$  and  $[\text{IP}_3]^{\text{sn2}} = 1.10 \mu\text{M}$  with saddle-node bifurcations at  $[\text{IP}_3]^{\text{sn1}}$  and  $[\text{IP}_3]^{\text{sn2}}$ . The central dashed curve indicates unstable fixed points, while the other dashed curves indicate unstable periodic orbits. The inset shows an enlargement of the region around the Hopf bifurcation at  $[\text{IP}_3] = [\text{IP}_3]^{\text{h1}}$ .

For such large diffusion coefficients,  $\text{Ca}^{2+}$  diffuses rapidly through the entire cell and couples the release clusters tightly. As a consequence,  $\text{Ca}^{2+}$  gradients and fluctuations are negligible and the system is expected to be described by the following system of ordinary differential equations (see also appendix B):

$$\begin{aligned} \frac{d[\text{Ca}^{2+}]}{dt} &= -v_P \frac{[\text{Ca}^{2+}]^2}{k^2 + [\text{Ca}^{2+}]^2} + (v_L + v_C m_\infty^3 n_\infty^3 h^3)([\text{Ca}^{2+}]_{\text{ER}} - [\text{Ca}^{2+}]) \\ \frac{dh}{dt} &= \alpha_h(1 - h) - \beta_h h, \end{aligned} \quad (7)$$

where the fraction of open channels  $N_{\text{open}}/N$  in equation (4) is replaced by the continuous activation variable  $h^3$ . These equations predict the bifurcation diagram, shown in figure 1. There is a subcritical Hopf bifurcation at  $[\text{IP}_3] = 0.2394 \mu\text{M} \equiv [\text{IP}_3]^{\text{h1}}$  and at  $[\text{IP}_3] = 0.82 \mu\text{M} \equiv [\text{IP}_3]^{\text{h2}}$ . The upper and lower branches indicate the minimum and maximum amplitudes of  $\text{Ca}^{2+}$  oscillations. Saddle-node bifurcations at  $[\text{IP}_3] = 0.2386 \mu\text{M} \equiv [\text{IP}_3]^{\text{sn1}}$  and  $[\text{IP}_3] = 1.10 \mu\text{M} \equiv [\text{IP}_3]^{\text{sn2}}$  terminate the oscillating branches. The central dashed curve indicates an unstable fixed point while the other dashed curves indicate unstable periodic orbits.

Similar to neurons, the information of the  $\text{Ca}^{2+}$  signal is mostly coded in the frequency of spikes. Thus, ER membranes with tightly coupled clusters only encode information when the concentration of  $\text{IP}_3$  is larger than the threshold of about  $0.24 \mu\text{M}$ . The assertion that the

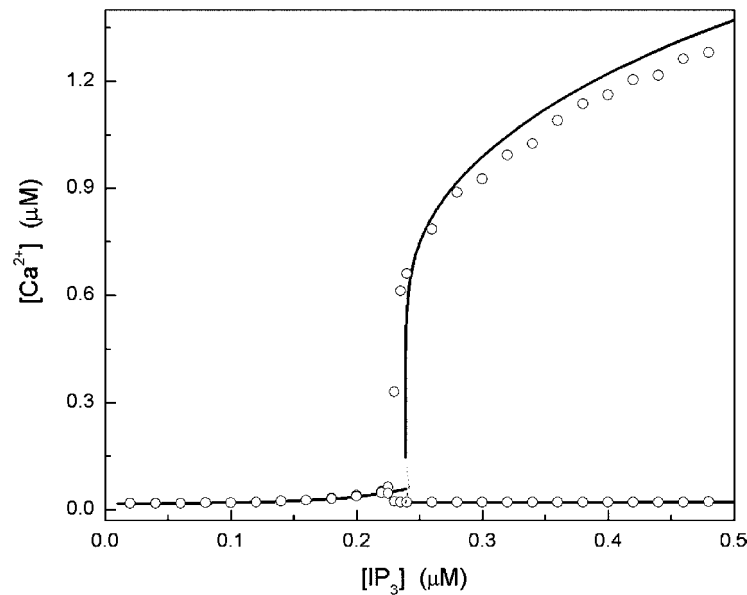


**Figure 2.** Minimum and maximum amplitudes of the  $\text{Ca}^{2+}$  signals are shown as a function of the  $\text{IP}_3$  concentration. Open circles indicate numerical solutions of the spatially explicit model (1) with a  $60 \mu\text{m} \times 60 \mu\text{m}$  cell with clusters of 36 channels at a distance of  $3 \mu\text{m}$  and  $D = 200 \mu\text{m}^2 \text{s}^{-1}$ . The full curve and dashed line (unstable periodic orbit) represents the predictions from equation (7).

gradients and spatial dependencies in equation (1) can be neglected in the case of a large  $\text{Ca}^{2+}$  diffusion coefficient is verified by comparing the cell-averaged response obtained from numerical solution of equation (1) ( $D = 200 \mu\text{m}^2 \text{s}^{-1}$ ) with that from the simpler spatially not explicit model in equation (7) in figure 2. In figure 3, we show samples of  $\text{Ca}^{2+}$  release of a single release cluster with  $N = 36$  channels embedded into a patch of the ER with a large diffusion coefficient (i.e. the gradient and inhomogeneous terms in equation (1) are neglected), described by

$$\frac{d[\text{Ca}^{2+}]}{dt} = -v_p \frac{[\text{Ca}^{2+}]^2}{k^2 + [\text{Ca}^{2+}]^2} + \left( v_L + v_C m_\infty^3 n_\infty^3 \frac{N_{\text{open}}}{N} \right) ([\text{Ca}^{2+}]_{\text{ER}} - [\text{Ca}^{2+}]) \quad (8)$$

where  $N_{\text{open}}/N$  is the fraction of open channels. The small number of channels  $N = 36$  requires stochastic modelling of the fraction of open channels. Similar as predicted by the homogeneous model (equation (7)) for large diffusion coefficients, the stochastic model (8) for the  $\text{Ca}^{2+}$  release from a single cluster predicts almost constant  $\text{Ca}^{2+}$  levels (with small fluctuations) well below the threshold of  $[\text{IP}_3]^{(\text{sn})}$ . For larger  $\text{IP}_3$  concentrations, noisy oscillations emerge. Most importantly, the  $\text{Ca}^{2+}$  signal does not code information for small  $\text{IP}_3$  concentrations.

#### 4. Sub-threshold coherent $\text{Ca}^{2+}$ oscillations

Lowering the  $\text{Ca}^{2+}$  diffusion coefficient towards physiological values, the coupling between the release clusters, facilitated by  $\text{Ca}^{2+}$  diffusion through the intracellular space, is decreased and the emergence of local  $\text{Ca}^{2+}$  release events is observed. This is demonstrated in the two panels of figure 4, where we compare the cell-averaged  $\text{Ca}^{2+}$ -signal for  $D = 20 \mu\text{m}^2 \text{s}^{-1}$

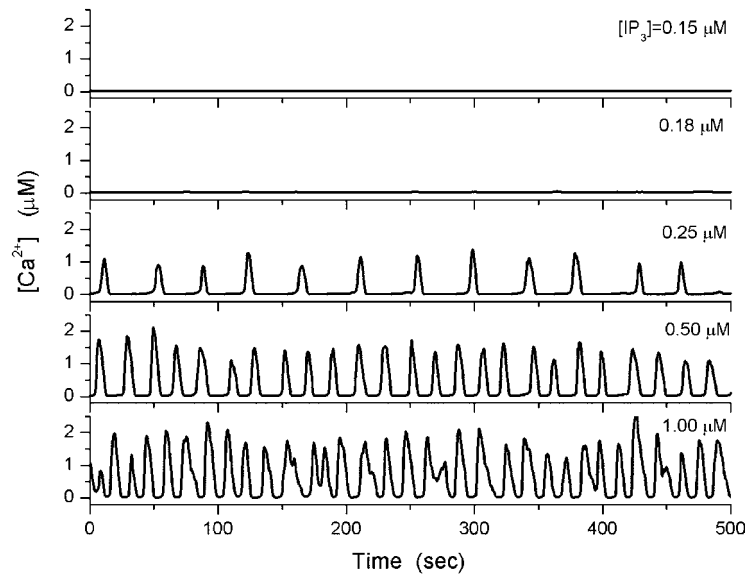


**Figure 3.** Trajectories of  $\text{Ca}^{2+}$  released by a single cluster of  $N = 36$   $\text{IP}_3$ Rs embedded in the ER membrane with continuously distributed pumps and leakage under the assumption of a large  $\text{Ca}^{2+}$  diffusion coefficient  $D$ .

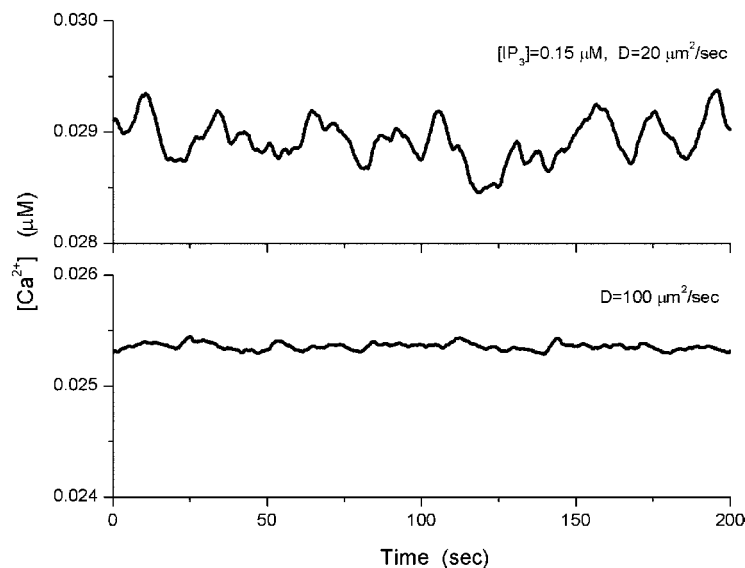


**Figure 4.**  $\text{Ca}^{2+}$  release as a function of time of the centre cluster of the cell at  $D = 20 \mu\text{m}^2 \text{s}^{-1}$  (upper panel) and  $D = 100 \mu\text{m}^2 \text{s}^{-1}$  (lower panel) for  $[\text{IP}_3] = 0.15 \mu\text{M} < [\text{IP}_3]^{\text{sn1}}$ , i.e. below the threshold of  $\text{Ca}^{2+}$  oscillations predicted by the deterministic model equation (7).

(upper panel) and  $D = 100 \mu\text{m}^2 \text{s}^{-1}$  (lower panel) at  $[\text{IP}_3] < [\text{IP}_3]^{\text{sn1}}$ , i.e. below the threshold of  $\text{Ca}^{2+}$  oscillations predicted by the deterministic model (7). The cell-averaged  $\text{Ca}^{2+}$  signal exhibits a larger spontaneous activity at the smaller diffusion coefficient. In figure 5 we show the minimum and maximum amplitudes of the calcium signals generated by the whole-cell model (1) as a function of  $[\text{IP}_3]$  for  $D = 20, 15, 10$  and  $5 \mu\text{m}^2 \text{s}^{-1}$ . For  $D = 20 \mu\text{m}^2 \text{s}^{-1}$  we observe—

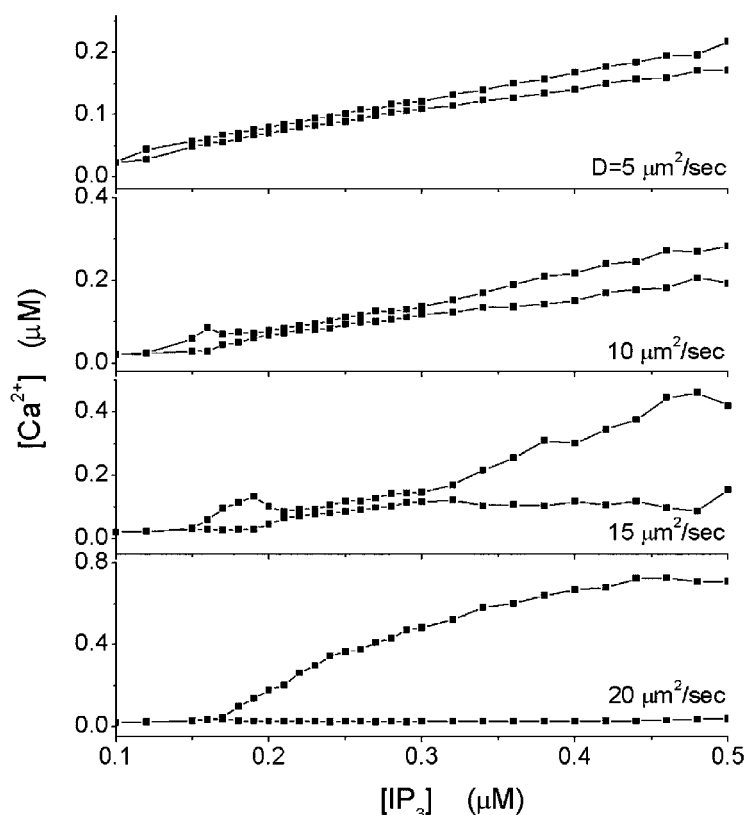


**Figure 5.** Minimum and maximum cell-averaged  $\text{Ca}^{2+}$  concentrations as a function of the  $\text{IP}_3$  concentrations for various values of the  $\text{Ca}^{2+}$  diffusion coefficient  $D$ . In the cell model, each release cluster comprises  $N = 36$  channels and the clusters are  $3 \mu\text{m}$  apart.

as expected—a smooth transition from the non-oscillatory to the oscillatory regime, smoothed by channel noise. Oscillations extend to concentrations of  $\text{IP}_3$  well below the deterministic threshold. For  $D = 15 \mu\text{m}^2 \text{s}^{-1}$  we observe that the oscillations occur in two distinctly different ranges of  $\text{IP}_3$  concentrations, one below the deterministic threshold (the small ‘bubble’ at  $0.15 \mu\text{M} < [\text{IP}_3] < 0.22 \mu\text{M}$ ) and one within the  $\text{IP}_3$  interval of oscillations predicted by (7) at  $[\text{IP}_3] > 0.3 \mu\text{M}$ . In figure 6 trajectories of the cell-averaged  $\text{Ca}^{2+}$  concentration and the  $\text{Ca}^{2+}$  concentration at the centre cluster are shown for concentrations of  $\text{IP}_3$  within this sub-threshold oscillatory regime and beyond.

The cell-averaged  $\text{Ca}^{2+}$  signal exhibits a large amplitude and a more coherent structure in the ‘bubble’ of sub-threshold oscillations as compared to concentrations of  $\text{IP}_3$  below and above the bubble (see the upper three panels in figure 6). For further decreasing  $D$ , the bubble of sub-threshold oscillations shifts to smaller values of the  $\text{IP}_3$  concentrations and becomes smaller in amplitude (see figure 5). The deterministically predicted supra-threshold oscillations (equation (7)) occur at larger concentrations of  $\text{IP}_3$  (see figure 5) and their amplitudes become smaller as  $D$  is decreased.

For  $D = 15 \mu\text{m}^2 \text{s}^{-1}$  the  $\text{Ca}^{2+}$  supra-threshold oscillations (at the centre cluster and cell-averaged) are shown in the fourth panels from above in figure 6. Comparing the second and the fourth panels (from above) in figure 6 one can see that the supra-threshold oscillations are less

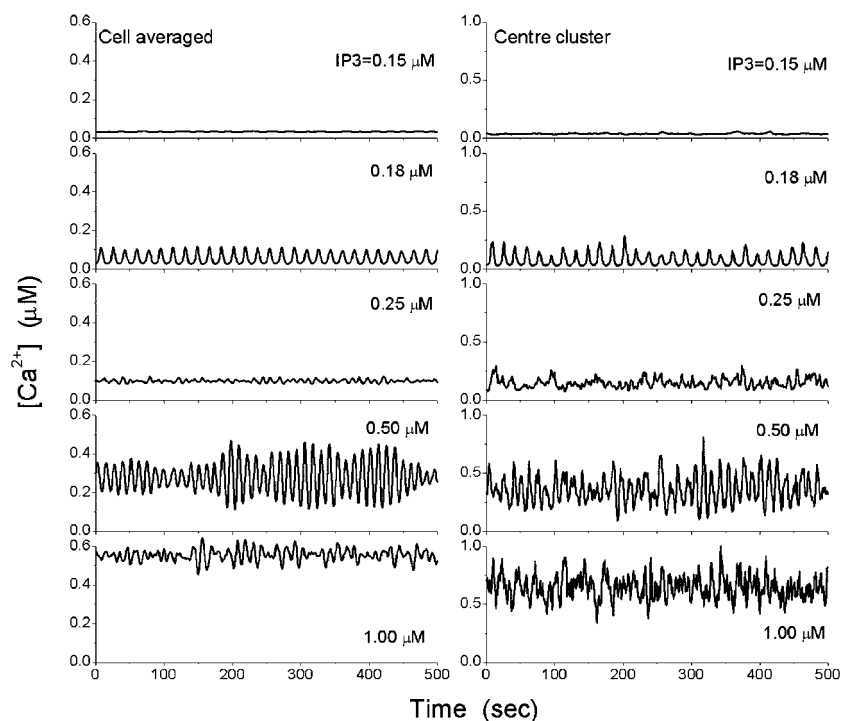


**Figure 6.** Trajectories of the cell-averaged Ca<sup>2+</sup> concentration (left panels) and the Ca<sup>2+</sup> concentration at the centre cluster (right panels) are shown for various concentrations of IP<sub>3</sub> at  $D = 15 \mu\text{m}^2 \text{s}^{-1}$ . In the cell model, each release cluster comprises  $N = 36$  channels and the clusters are  $3 \mu\text{m}$  apart.

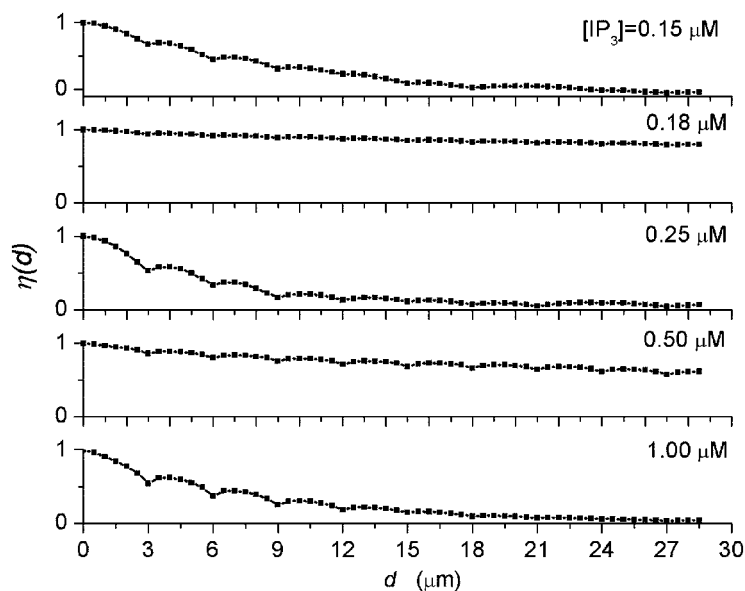


**Figure 7.** Cross-correlation function equation (9) between the Ca<sup>2+</sup> release at the centre cluster and sites at increasing distance are shown at various concentrations of IP<sub>3</sub>. The clusters each comprise 36 channels and are  $3 \mu\text{m}$  apart from each other.

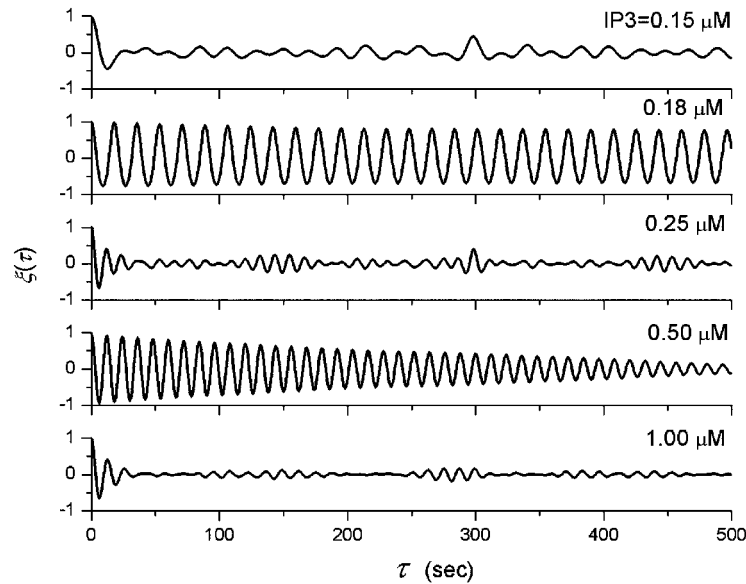


**Figure 8.** The normalized autocorrelation functions equation (10) of the  $\text{Ca}^{2+}$  concentration at the centre cluster are shown at various concentrations of  $\text{IP}_3$ . The clusters each comprise 36 channels and are  $3 \mu\text{m}$  apart from each other.

coherent in time although larger in amplitude. Figure 7 shows the normalized cross-correlation function between the  $\text{Ca}^{2+}$  concentrations at the central release cluster  $[\text{Ca}](0, t)$  and a distance  $d$  away from the centre cluster  $\text{Ca}^{2+}(d, t)$ , i.e.

$$\eta(d) = \frac{\int_0^T (C(t, 0) - \langle C(0) \rangle)(C(t, d) - \langle C(d) \rangle) dt}{\sqrt{\int_0^T (C(t, 0) - \langle C(0) \rangle)^2 dt \int_0^T (C(t, d) - \langle C(d) \rangle)^2 dt}} \quad (9)$$

where  $C(t, 0) \equiv [\text{Ca}^{2+}](0, t)$  and  $C(t, d) \equiv [\text{Ca}^{2+}](d, t)$ . While the correlations decay rapidly for  $[\text{IP}_3] = 0.15 \mu\text{M}$ , they decay much more slowly at the maximum of the ‘bubble’ (at  $[\text{IP}_3] = 0.18 \mu\text{M}$ ) and decay rapidly again at  $[\text{IP}_3] = 0.25 \mu\text{M}$ . Thus, the temporally coherent sub-threshold oscillations (within the bubble) are also spatially coherent. The spatial coherence increases again for larger concentrations of  $\text{IP}_3$  where supra-threshold oscillations occur to a lesser degree as the sub-threshold oscillations (compare the third panel from above (supra-threshold) in figure 7 with the second panel from above (sub-threshold)). Temporal correlations are described by the normalized autocorrelation function of the  $\text{Ca}^{2+}$  release at a release site (we picked the centre site)

$$\xi(\tau) = \frac{\int_0^T (C(t) - \langle C \rangle)(C(t + \tau) - \langle C \rangle) dt}{\int_0^T (C(t) - \langle C \rangle)^2 dt}, \quad (10)$$

where  $C(t)$  denotes the  $\text{Ca}^{2+}$  concentration at a release site and  $\langle C(t) \rangle$  the temporally averaged  $\text{Ca}^{2+}$  concentration at this site. In figure 8, the normalized autocorrelation functions are shown for various  $\text{IP}_3$  concentrations including those where sub-threshold oscillations occur. The longest temporal correlations are observed at  $[\text{IP}_3] = 0.18 \mu\text{M}$ , i.e. where the sub-threshold oscillations have the largest amplitude. It is remarkable that the temporal correlations of the

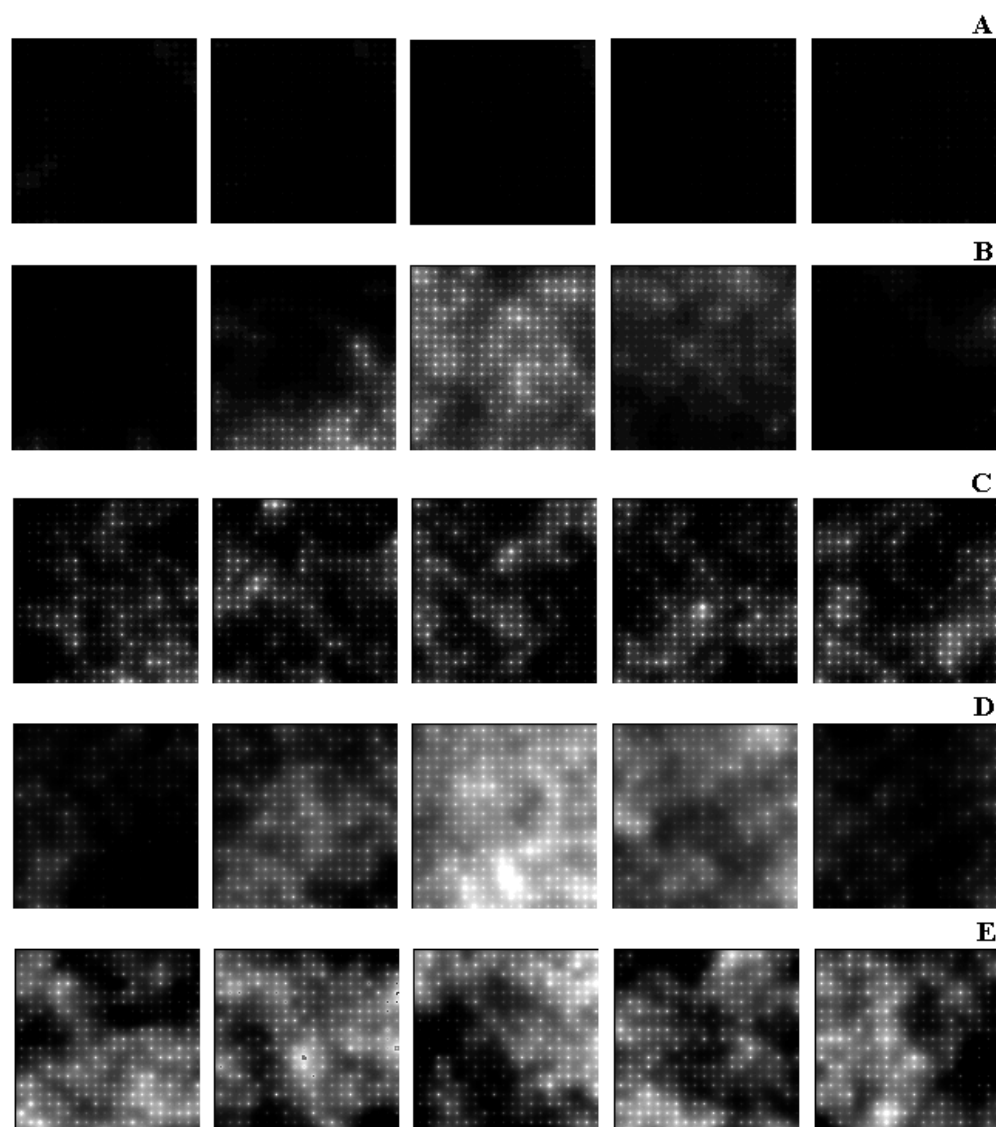


**Figure 9.** Snapshots of the  $\text{Ca}^{2+}$  concentrations in the cell are shown at  $[\text{IP}_3] = 0.15 \mu\text{M}$  (A),  $0.18 \mu\text{M}$  (B),  $0.25 \mu\text{M}$  (C),  $0.5 \mu\text{M}$  (D), and  $1.00 \mu\text{M}$  (E). The time interval between the snapshots is 3 s. The cell has the dimensions  $60 \mu\text{m} \times 60 \mu\text{m}$  and comprises clusters with  $N = 36$  channels at a distance of  $3 \mu\text{m}$ . Lighter grey indicates a higher  $\text{Ca}^{2+}$  concentration.

supra-threshold oscillations ( $[\text{IP}_3] = 0.5 \mu\text{M}$ ) (see figure 8) are shorter than those of the sub-threshold oscillations.

The strongly enhanced spatiotemporal coherence of the sub-threshold oscillations can be seen in the snapshots of the  $\text{Ca}^{2+}$  concentration of the 2D whole-cell model shown in figure 9. Each row in figure 9 represents a sequence of snapshots (each 3 s apart) at a different  $\text{IP}_3$  concentration. Lighter grey indicates a higher  $\text{Ca}^{2+}$  concentration. While only  $\text{Ca}^{2+}$  puffs (localized release events) can be seen for  $[\text{IP}_3] = 0.15 \mu\text{M}$ , temporally and spatially coherent oscillations are observed at  $[\text{IP}_3] = 0.18 \mu\text{M}$  (i.e. at the maximum of the bubble of sub-threshold

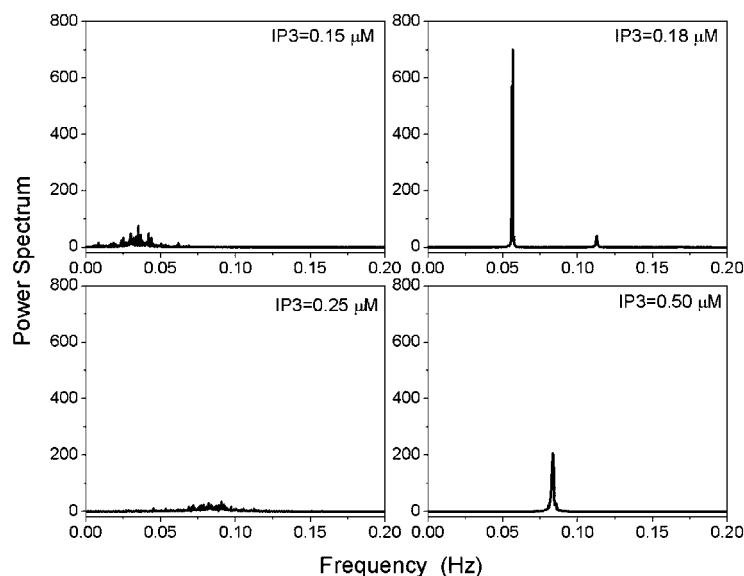


**Figure 10.** Power spectra of the cell-averaged  $\text{Ca}^{2+}$  signal at  $D = 15 \mu\text{m}^2 \text{s}^{-1}$  and  $[\text{IP}_3] = 0.15, 0.18, 0.25$  and  $0.5 \mu\text{M}$ . The cell's dimension is  $60 \mu\text{m} \times 60 \mu\text{m}$ , the cluster distance is  $3 \mu\text{m}$  and each cluster comprises 36 channels.

oscillations). The  $\text{Ca}^{2+}$  activity for  $[\text{IP}_3] = 0.25 \mu\text{M}$  is again spatially and temporally less coordinated across the cell. At an  $\text{IP}_3$  concentration of  $0.5 \mu\text{M}$ , the coherence is enhanced again due to the onset of supra-threshold oscillations.

From a physiological point of view, the actual frequency of the oscillations is of great relevance since it encodes information. In figure 10 we show power spectra of the cell-averaged  $\text{Ca}^{2+}$  signal at  $D = 15 \mu\text{m}^2 \text{s}^{-1}$  and  $\text{IP}_3$  concentrations that include the regime of sub-threshold oscillations. The power spectrum exhibits strong peaks (fundamental and higher harmonics) when sub-threshold oscillations are observed. These peaks are higher and sharper than those for supra-threshold oscillations (see panel for  $[\text{IP}_3] = 0.5 \mu\text{M}$ ). In figure 11 we show the base-frequency and peak height as a function of  $[\text{IP}_3]$ . In the regime of optimal sub-threshold oscillations (i.e.  $[\text{IP}_3] \approx 0.18 \mu\text{M}$ ) the frequency is lower than for supra-threshold oscillations and the peak height is larger by almost one order of magnitude, underpinning the dramatic coherence of the sub-threshold oscillations. The frequency first increases with increasing  $\text{IP}_3$  concentration and then slowly decreases towards the frequency of the spatially homogeneous (i.e. noise-free) model (7).

## 5. Optimal clustering

Related to the coherent sub-threshold oscillations described in the previous section is the occurrence of optimal clustering [35]. We consider the case of small  $\text{IP}_3$  concentrations, i.e.  $[\text{IP}_3] < 0.24 \mu\text{M}$ , corresponding to a situation where only few agonist molecules are binding. Given that the typical cluster distance in *Xenopus* oocyte is about  $3 \mu\text{m}$  and that there are about 20–40 channels/cluster, our  $60 \mu\text{m} \times 60 \mu\text{m}$  size cell comprises 12 000–16 000 release channels and we pick 14 400 [35]. Given this fixed total number, we seek to find the optimal geometric configuration of these channels in order to achieve the best signalling response to stimulation by

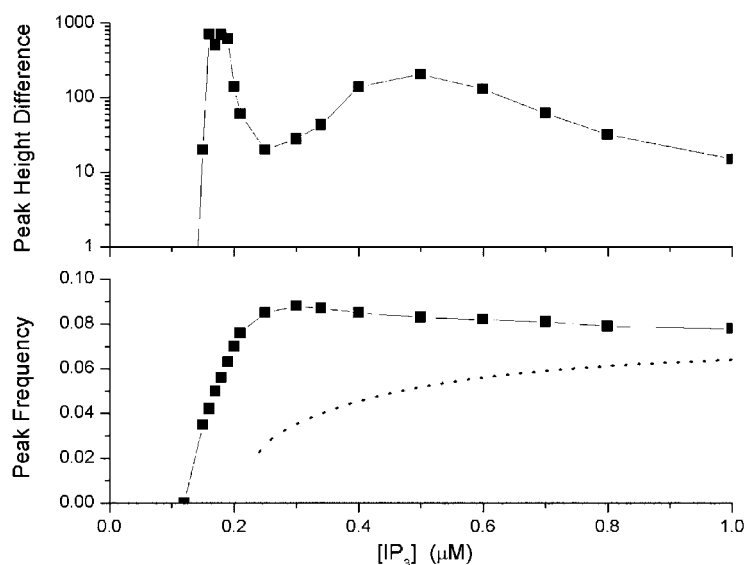


**Figure 11.** The base frequency (lower panel) and peak heights (upper panel) in the power spectra of the cell-averaged  $\text{Ca}^{2+}$  concentration are shown as a function of the  $\text{IP}_3$  concentration. The cell's dimension is  $60 \mu\text{m} \times 60 \mu\text{m}$ , the cluster distance is  $3 \mu\text{m}$  and each cluster comprises 36 channels. The dashed curve represents the frequency of the  $\text{Ca}^{2+}$  oscillations predicted by the homogeneous model equation (7).

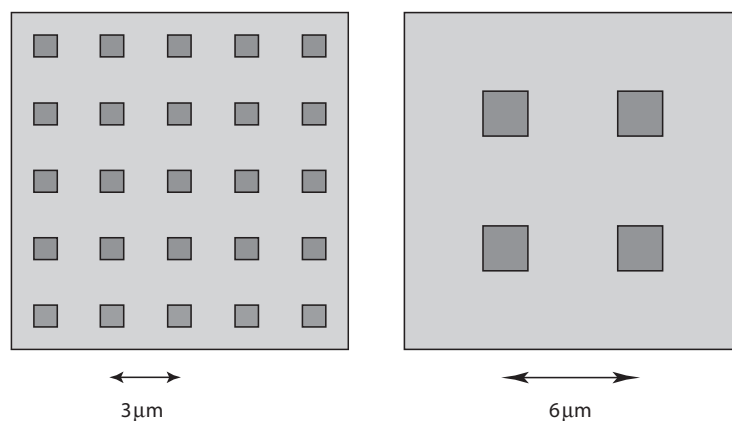


**Figure 12.** Sketches of two possible configurations of  $\text{IP}_3\text{Rs}$  are shown as examples. In the left panel, the clusters are  $3 \mu\text{m}$  apart and each contain 36 channels. In the right panel each cluster contains 144 channels and their distance is  $6 \mu\text{m}$ .

a small concentration of  $\text{IP}_3$ . The configurations we choose from are square arrays of clusters of release channels with different numbers of channels per cluster and cluster distances so that the total number of channels is conserved (see figure 12 for two possible configurations).

We start with single channels distributed homogeneously at a distance of  $d = 0.5 \mu\text{m}$  over a cell, i.e. in  $120 \times 120$  clusters of single channels ( $N = 1$ ) at a physiological diffusion coefficient

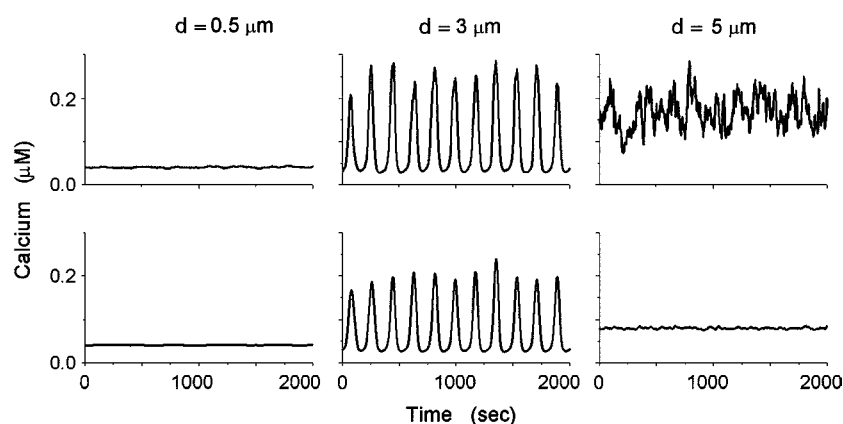


**Figure 13.** The time traces of the  $\text{Ca}^{2+}$  concentrations at active sites are shown in the upper panels for cluster distances of  $d = 0.5 \mu\text{m}$  (homogeneous channel distribution),  $d = 3$  and  $5 \mu\text{m}$  (from left to right). The lower panels show the corresponding cell-averaged  $\text{Ca}^{2+}$  signals. For all panels we used the parameters  $[\text{IP}_3] = 0.21 \mu\text{M}$  and  $D = 20 \mu\text{m}^2 \text{s}^{-1}$ .

of  $D = 20 \mu\text{m}^2 \text{s}^{-1}$  and  $[\text{IP}_3] = 0.21 \mu\text{M}$ . The  $\text{Ca}^{2+}$  traces shown in the upper left panel in figure 13 are obtained from a cluster site. The panel below it depicts the cell-averaged  $\text{Ca}^{2+}$  concentration. The cell-averaged  $\text{Ca}^{2+}$  signal does not exhibit spikes that could be interpreted as a signal in response to the stimulation by  $\text{IP}_3$ . In the next step we increase the distance  $d$  of the clusters of the  $\text{IP}_3\text{Rs}$  to  $3 \mu\text{m}$  but increase their sizes to  $N = 36$  channels so that the total number of channels remains 14 400. A trace of  $\text{Ca}^{2+}$  taken at a cluster site is shown in the central upper panel in figure 13. The panel below it shows the cell-averaged  $\text{Ca}^{2+}$  concentration. The cell-averaged  $\text{Ca}^{2+}$  response as well as that at a single release site is almost periodic with an amplitude that is orders of magnitude larger than in the previously discussed case where the cluster distance was only  $0.5 \mu\text{m}$ . Increasing the distance between the clusters further to  $5 \mu\text{m}$  with a cluster size of  $N = 100$  channels results again in a stochastic  $\text{Ca}^{2+}$  signal (see upper right panel in figure 13). The cell-averaged  $\text{Ca}^{2+}$  signal is temporally incoherent. Thus, similar as for  $d = 0.5 \mu\text{m}$ , the cell cannot produce a global  $\text{Ca}^{2+}$  signal upon weak stimulation with  $\text{IP}_3$ .

To describe the capability of the cellular  $\text{Ca}^{2+}$  signalling mechanism we plot the minimum and maximum amplitudes of the computed cell-averaged  $\text{Ca}^{2+}$  concentrations as a function of the cluster distance in figure 14 at the sub-threshold  $\text{IP}_3$  concentration of  $0.21 \mu\text{M}$  at various values of the  $\text{Ca}^{2+}$  diffusion coefficient  $D$ . Large gaps between minimum and maximum amplitudes in figure 14 correlate with spatiotemporal coherence as shown in figure 15. For small and large cluster distances, minimum and maximum amplitudes are very close, i.e. the cell is not capable of signalling upon the weak stimulation of  $\text{IP}_3$ . In between, we find intervals of cluster distances at which the cell is capable of generating large amplitude and coherent  $\text{Ca}^{2+}$  signals that may be decoded in the cell to trigger downstream processes. At physiological values of  $D \approx 20\text{--}30 \mu\text{m}^2 \text{s}^{-1}$  optimal cluster distances are predicted by the model at about  $3 \mu\text{m}$  which agrees with measured average cluster distances of *Xenopus* oocyte [36]. A cluster distance of  $3 \mu\text{m}$  corresponds to a cluster size of 36 channels, which is well in the range of estimated values at *Xenopus* oocyte [6]. In figure 16, we show minimum and maximum amplitudes of the cell-averaged  $\text{Ca}^{2+}$  signals at the supra-threshold concentrations of  $[\text{IP}_3] = 0.25 \mu\text{M}$ . Above the

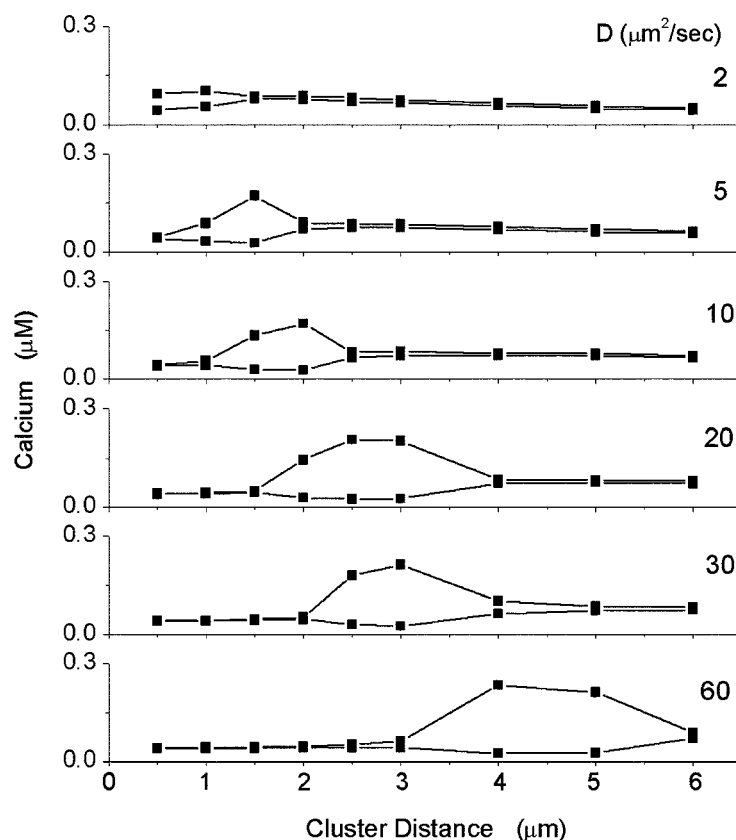


**Figure 14.** The minimum and maximum amplitudes of the cell-averaged  $\text{Ca}^{2+}$  are shown as a function of the cluster distance at various values of  $D$  at an  $\text{IP}_3$  concentration of  $0.21 \mu\text{M}$ . Large gaps between the minimum and the maximum amplitudes indicate a signal of large amplitude. In the same intervals, the cell-averaged  $\text{Ca}^{2+}$  signal is also temporally coherent and the clusters are phase synchronized (see figure 15 and [35]).

oscillation threshold of  $[\text{IP}_3] = 0.24 \mu\text{M}$ , the bubbles are of optimal extent to the homogeneous distribution of clusters. Clustering here has no enhancing effect on encoding an  $\text{IP}_3$  signal (see figure 16).

## 6. Discussion and conclusion

Using mathematical modelling, we have demonstrated dramatic changes in intracellular calcium signalling patterns due to clustering of the  $\text{IP}_3$  receptors. The dynamic behaviour of  $\text{Ca}^{2+}$  release from internal stores predicted for homogeneous distributions of  $\text{IP}_3$  receptors is altered most dramatically at low concentrations of the second messenger  $\text{IP}_3$ . Our model, incorporating physiologically meaningful values for the size of the cluster and their spacing, predicts a range of sub-threshold  $\text{IP}_3$  concentrations at which the cell responds extremely coherently and thus codes effectively for the  $\text{IP}_3$  signal. We have also shown that a homogeneous distribution of channels in the same regime would not result in a coherent cellular  $\text{Ca}^{2+}$  signal and thus would not permit coding of the weak  $\text{IP}_3$  signal. The effect is due to synergetic interaction of channel fluctuations and geometric distribution of the channels in clusters.

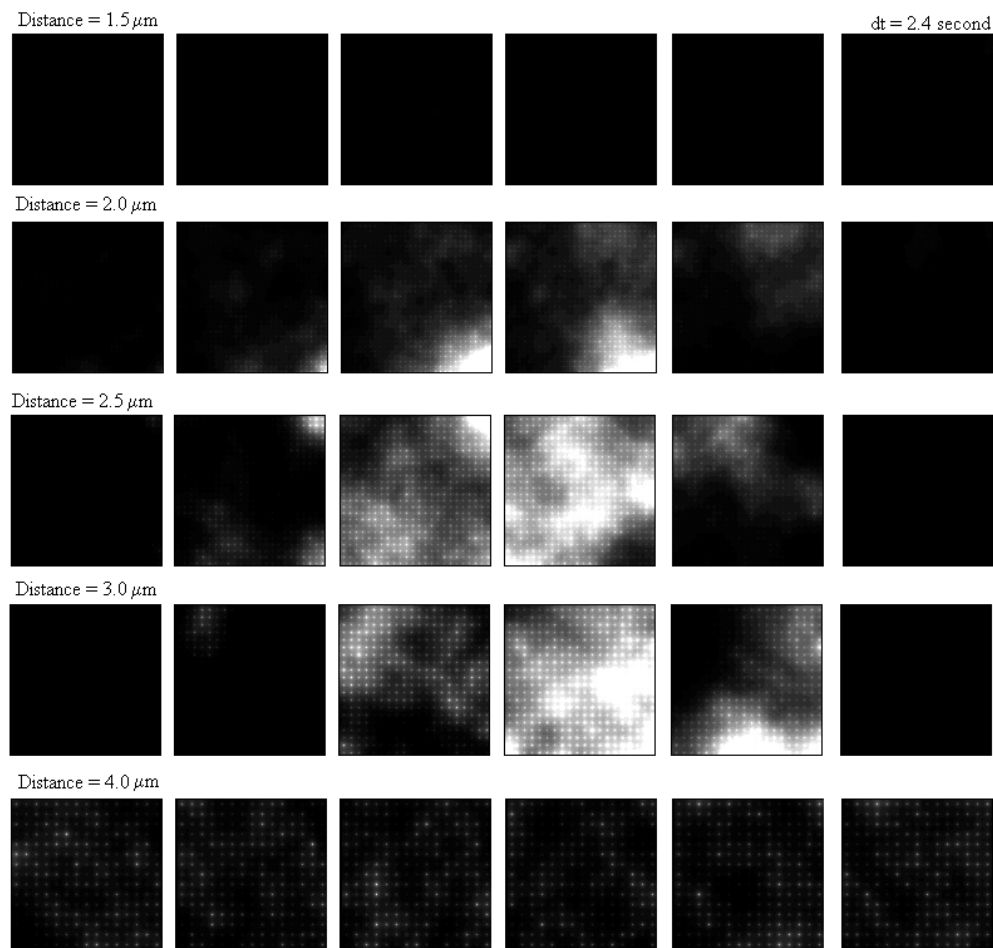


**Figure 15.** Snapshots of the  $\text{Ca}^{2+}$  concentration are shown at a cluster–cluster distance of  $1.5 \mu\text{m}$  (top row),  $2.0 \mu\text{m}$  (second row from top),  $2.5 \mu\text{m}$  (third row from top),  $2.5 \mu\text{m}$  (third row from top),  $3.0 \mu\text{m}$  (fourth row from top),  $4.0 \mu\text{m}$  (bottom row from top) at  $[\text{IP}_3] = 0.21 \mu\text{M}$  and  $D = 20 \mu\text{m}^2 \text{s}^{-1}$ . Each snapshot has a size of  $60 \mu\text{m} \times 60 \mu\text{m}$ . The grey scales from black to white represent  $\text{Ca}^{2+}$  concentration from  $0.05$  to  $0.25 \mu\text{M}$ .

What is most remarkable and surprising is that the temporal and spatial correlations of this additional branch of  $\text{Ca}^{2+}$  oscillations exhibits a larger temporal and spatial coherence than those oscillations predicted for a homogeneous distribution of  $\text{IP}_3$ Rs at larger values of  $\text{IP}_3$  concentration. The spatial and temporal coherence of the cellular  $\text{Ca}^{2+}$  signal correlates with a coherent spatiotemporal  $\text{Ca}^{2+}$  wave that can trigger other downstream processes, including modification of gene regulatory networks, and is thus of physiological relevance.

While many oscillatory and excitable models that predict pattern formation have been published in the context of fluid dynamics, chemical reactions and membrane physiology, most of them are spatially homogeneous. In the type of model we are discussing here (see also recent work by [24] and [25]), the active sites, responsible for the pattern formation, are distributed in small clusters, often not bigger than  $0.1 \mu\text{m}$  and a few microns apart. The smallness of these clusters not only influences the spatiotemporal patterns by their geometrically heterogeneous

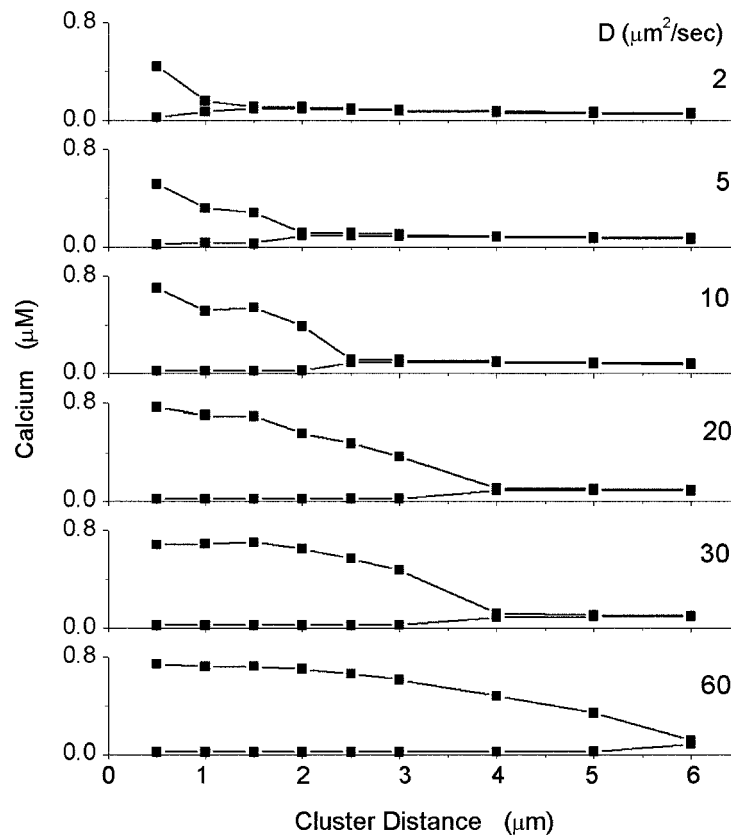


**Figure 16.** The minimum and maximum amplitudes of the cell-averaged  $\text{Ca}^{2+}$  signals are shown as a function of the cluster distance at  $[\text{IP}_3] = 0.25 \mu\text{M}$ . The  $\text{Ca}^{2+}$  signal present at small cluster distances disappears when the clusters become too far apart to synchronize.

distribution, but also generates strong local fluctuations due to thermal motion of the receptor proteins resulting in stochastic fluxes. A strongly clustered distribution of excitability changes the spatiotemporal properties of the nonlinear waves dramatically at realistic physiological values of the diffusion coefficient of  $\text{Ca}^{2+}$ . A wealth of novel pattern formation phenomena has emerged out of this type of system (some of which are described in this paper) that are being currently explored computationally but are not well understood conceptually.

### Acknowledgment

This material is based upon work supported by the National Science Foundation under Grant No IBN-0078055.

### Appendix A. The stochastic calcium flux density through clustered $\text{IP}_3\text{Rs}$ (equation (4))

For one open  $\text{IP}_3\text{R}$  channel, the flux density can be expressed as

$$J_1 = v_{\text{IP}_3\text{R}} m_\infty^3 n_\infty^3 ([\text{Ca}^{2+}]_{\text{ER}} - [\text{Ca}^{2+}]) \quad (11)$$

where  $v_{IP_3R}$  denotes the maximum conductance. If the size of the channel is given by  $S_{IP_3R}$ , the total calcium flux through one open channel is given by

$$\bar{J}_1 = S_{IP_3R} J_1 = v_{IP_3R} S_{IP_3R} m_\infty^3 n_\infty^3 ([Ca^{2+}]_{ER} - [Ca^{2+}]). \quad (12)$$

The total flux through a cluster of  $N$  channels with  $N_{open}$  channels open then reads

$$\begin{aligned} \bar{J}_N &= N_{open} \bar{J}_1 \\ &= v_{IP_3R} S_{IP_3R} m_\infty^3 n_\infty^3 N_{open} ([Ca^{2+}]_{ER} - [Ca^{2+}]). \end{aligned} \quad (13)$$

In our simulations, each cluster is localized as a point source on a single grid element, with size  $\delta x^2$  ( $\delta x = 0.5 \mu m$ ). Thus the flux density of  $Ca^{2+}$  at a single grid is given by

$$\begin{aligned} J_{channel} &= \frac{\bar{J}_N}{\delta x^2} \\ &= v_c m_\infty^3 n_\infty^3 N_{open} ([Ca^{2+}]_{ER} - [Ca^{2+}]) \end{aligned} \quad (14)$$

with

$$v_c = \frac{S_{IP_3R}}{\delta x^2} v_{IP_3R} \quad (15)$$

which contains the ratio of channel size and grid size.

### Appendix B. The deterministic calcium flux density through $IP_3Rs$ (equation (7))

Suppose the cell has a size of  $S_{cell}$  and  $M$   $IP_3R$  channels distributed in it. With a large diffusion coefficient  $D$ ,  $Ca^{2+}$  diffuses rapidly through the entire cell and couples all the release channels tightly. As a consequence, calcium gradients and fluctuations can be ignored and the system can be treated as a point model. For this point model, the total  $Ca^{2+}$  flux through  $M_{open}$  open channels is given by (see equation (12))

$$\bar{J}_{cell} = M_{open} \bar{J}_1. \quad (16)$$

The flux density of  $Ca^{2+}$  is then obtained as

$$\begin{aligned} J_{cell} &= \frac{\bar{J}_{cell}}{S_{cell}} \\ &= v_{cell} m_\infty^3 n_\infty^3 \frac{M_{open}}{M} ([Ca^{2+}]_{ER} - [Ca^{2+}]) \end{aligned} \quad (17)$$

with

$$v_{cell} = v_c \frac{\delta x^2}{S_{cell}} M = \frac{M}{S_{cell}} S_{IP_3R} v_{IP_3R}. \quad (18)$$

For our particular choices of  $M = 14400$ ,  $\delta x = 0.5 \mu m$ , and  $S_{cell} = 60 \times 60 \mu m^2$ , i.e. one channel per grid element in the average, we find

$$J_{cell} = v_c m_\infty^3 n_\infty^3 h^3 ([Ca^{2+}]_{ER} - [Ca^{2+}]). \quad (19)$$

## References

- [1] Berridge M J, Bootman M D and Lipp P 1998 *Nature* **395** 645
- [2] Dolmetsch R E, Xu K and Lewis R S 1998 *Nature* **392** 933
- [3] Li W, Llopis J, Whitney M, Zlokarnik G and Tsien R Y 1998 *Nature* **392** 936
- [4] Cheng H, Lederer W J and Cannel M B 1993 *Science* **262** 740
- [5] Yao Y, Choi J and Parker I 1995 *J. Physiol. (Lond.)* **482** 533
- [6] Swillens S, Dupont G, Combettes L and Champeil P 1999 *Proc. Natl Acad. Sci. USA* **96** 13750
- [7] Yin C C and Lai F A 2000 *Nat. Cell* **2** 669
- [8] Sun X, Callamaras N, Marchant J S and Parker I 1998 *J. Physiol. (Lond.)* **509** 67
- [9] Thomas D, Lipp P, Berridge M J and Bootman M D 1998 *J. Biol. Chem.* **273** 27130
- [10] Callamaras N and Parker I 2000 *EMBO J.* **19** 3608
- [11] Marchant J S and Parker I 2001 *EMBO J.* **20** 65
- [12] Jouaville L S, Ichas F, Holmuhamedov E L, Camacho P and Lechleiter J D 1995 *Nature* **377** 438
- [13] Lechleiter J D, John L M and Camacho P 1998 *Biophys. Chem.* **72** 123
- [14] Cornell-Bell A H, Finkbeiner S M, Cooper M S and Smith S J 1990 *Science* **247** 470
- [15] Bootman M, Niggli E, Berridge M and Lipp P 1997 *J. Physiol. (Lond.)* **499** 307
- [16] Horne J H and Meyer T 1997 *Science* **276** 1690
- [17] Atri A, Amundson J, Clapham D and Sneyd J 1993 *Biophys. J.* **65** 1727
- [18] Kupferman R, Mitra P P, Hohenberg P D and Wang S S H 1997 *Biophys. J.* **72** 2430
- [19] Mckenzie A and Sneyd J 1998 *Int. J. Bifurcation Chaos* **8** 2003
- [20] Roth B J, Yagodin S V, Holtzclaw L and Russell J T 1995 *Cell Calcium* **17** 53
- [21] Bugrim A E, Zhabotinsky A M and Epstein I R 1997 *Biophys. J.* **73** 2897
- [22] Keizer J, Smith G D, Ponce-Dawson S and Pearson J E 1998 *Biophys. J.* **75** 595
- [23] Dawson S P, Keizer J and Pearson J E 1999 *Proc. Natl Acad. Sci. USA* **96** 6060
- [24] Keizer J and Smith G D 1998 *Biophys. Chem.* **72** 87
- [25] Falcke M, Tsimring L and Levine H 2000 *Phys. Rev. E* **62** 2636
- [26] De Young G W and Keizer J 1992 *Proc. Natl Acad. Sci. USA* **89** 9895
- [27] Falcke M 2003 *Biophys. J.* **84** 28  
Falcke M 2003 *Biophys. J.* **84** 42
- [28] Li Y and Rinzel J 1994 *J. Theor. Biol.* **166** 461
- [29] Shuai J W and Jung P 2002 *Biophys. J.* **83** 87
- [30] Shuai J W and Jung P 2002 *Phys. Rev. Lett.* **88** 681021
- [31] Shuai J W and Jung P 2003 *Function and Regulation of Cellular Systems: Experiments and Models* ed A Deutsch, J Howard, M Falcke and W Zimmerman (New York: Springer) at press
- [32] Shuai J W and Jung P 2003 *Phys. Rev. E* **67** 031905
- [33] Schneidman E, Freedman B and Segev I 1998 *Neural Comput.* **10** 1679
- [34] Albritton N L, Meyer T and Streyer L 1992 *Science* **258** 1812
- [35] Shuai J W and Jung P 2003 *Proc. Natl Acad. Sci. USA* **100** 506
- [36] Parker I, private communication